Supplemental

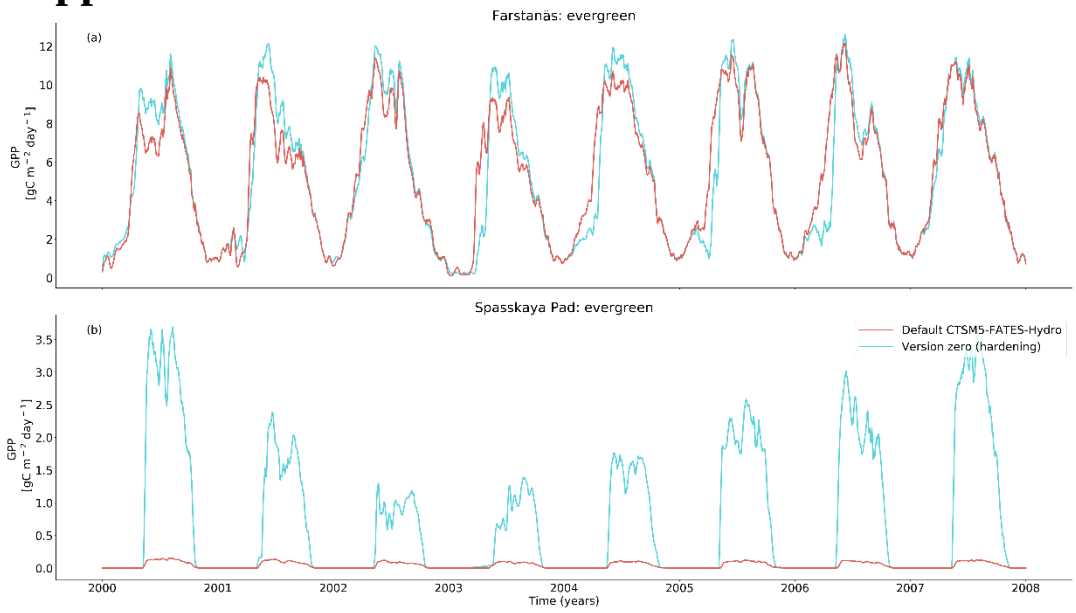

Figure S1: Gross primary productivity for needleleaf evergreen trees at the sites of a) Farstanäs, and b) Spasskaya Pad, during the period 2000-2008. The default simulation is shown in red, and the hardening simulation is shown in blue.

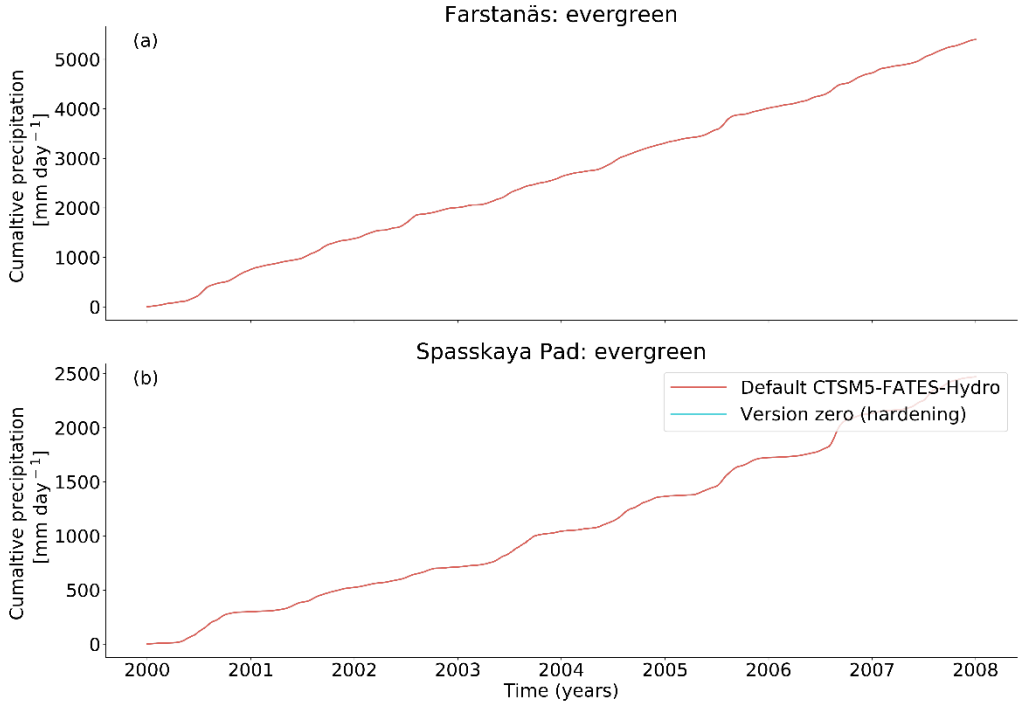

Figure S2: Cumulative total precipitation for needleleaf evergreen trees at the sites of a) Farstanäs, and b) Spasskaya Pad, during the period 2000-2008. The default simulation is shown in red, and the hardening simulation is shown in blue.

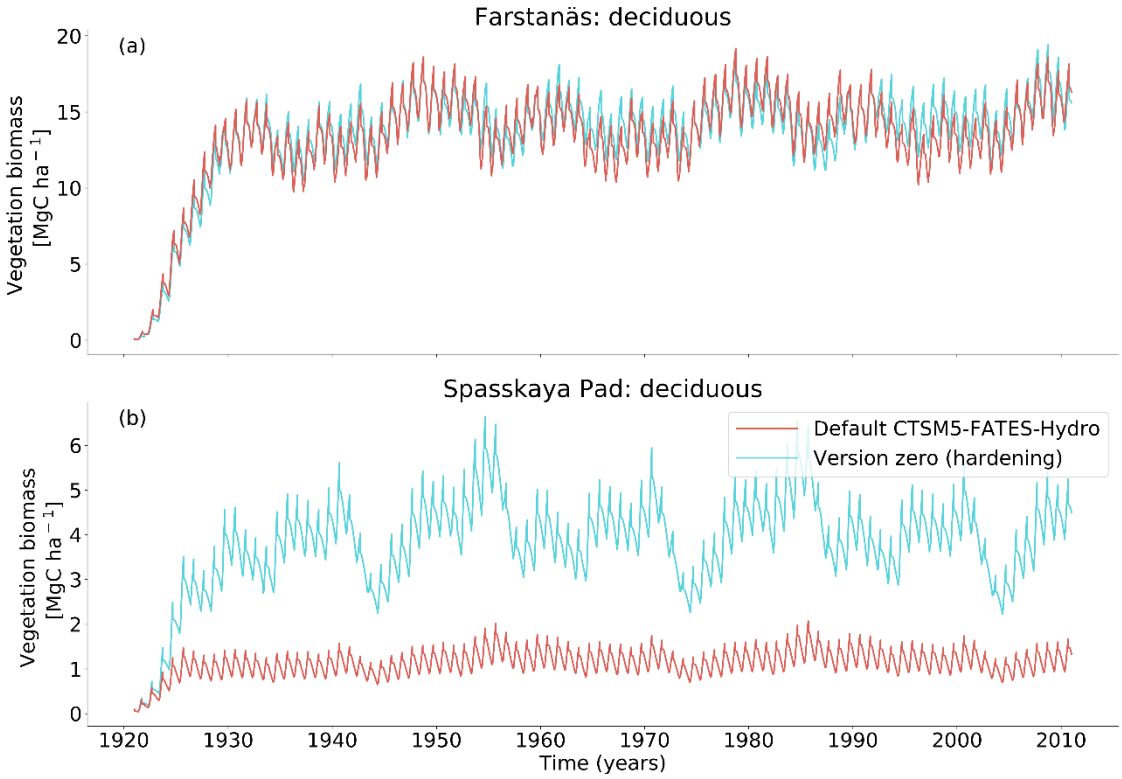

Figure S3: Living biomass for broadleaf deciduous trees at the sites of a) Farstanäs, and b) Spasskaya Pad, during the period 1921-2011 (atmospheric forcing: 3*[1981-2011]). The default simulation is shown in red, and the hardening simulation is shown in blue.

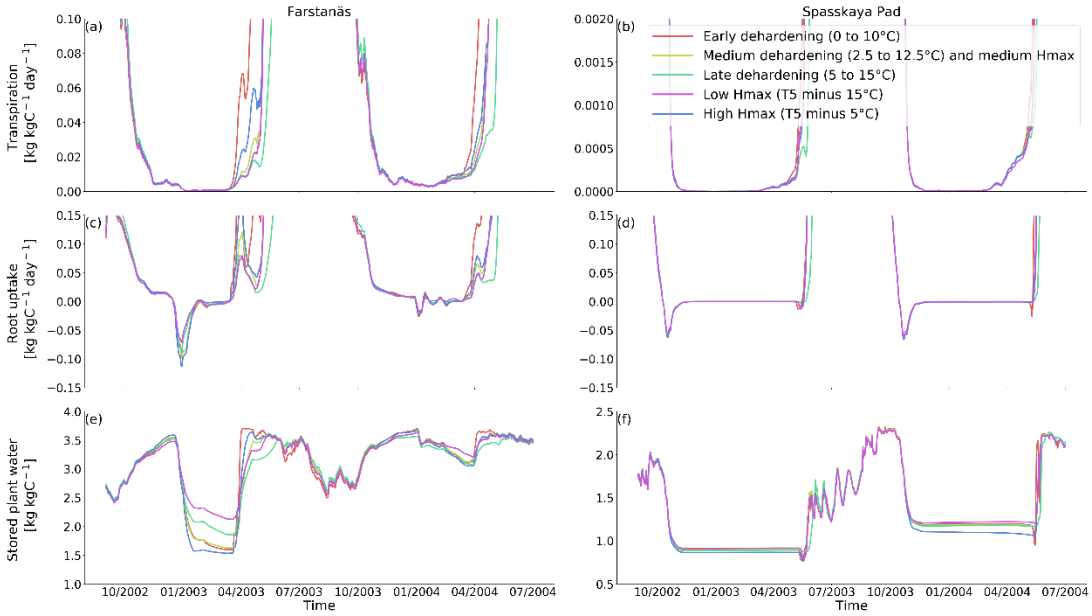

Figure S4: Plant water fluxes from dehardening and maximum hardiness level sensitivity analysis simulations for needleleaf evergreen trees at the sites of: Left) Farstanäs, and Right) Spasskaya Pad, during the period 2002/09-2004/07. Top: transpiration, middle: root water uptake, and bottom: stored plant water.

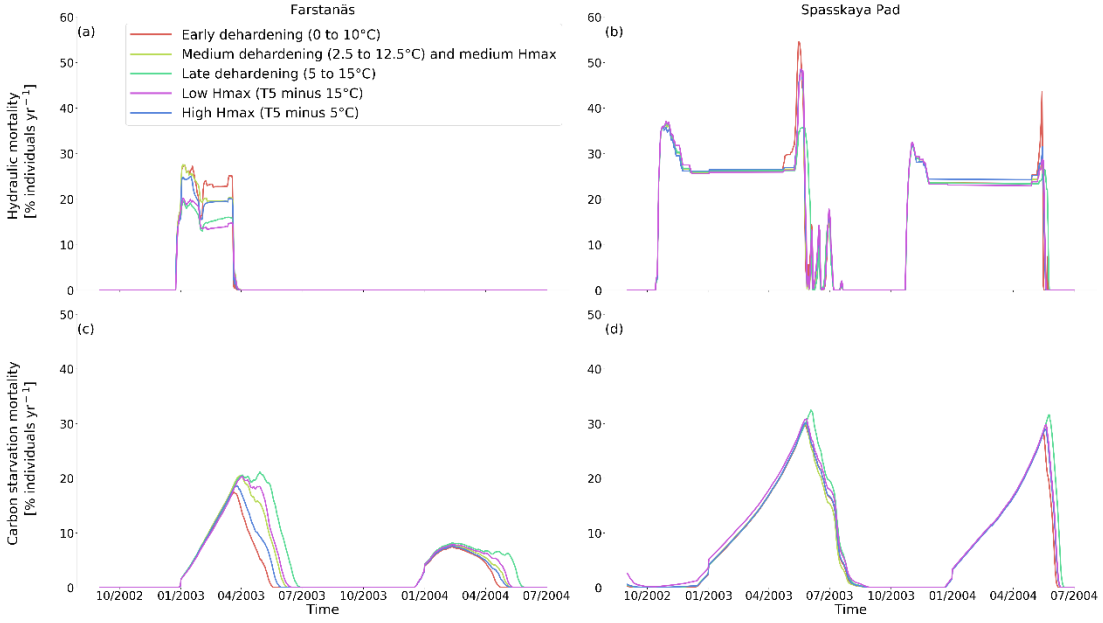

Figure S5: Mortality rates from dehardening and maximum hardiness level sensitivity analysis simulations for needleleaf evergreen trees at the sites of: Left) Farstanäs, and Right) Spasskaya Pad, during the period 2002/09-2004/07. Top: hydraulic failure mortality, and bottom: carbon starvation mortality.

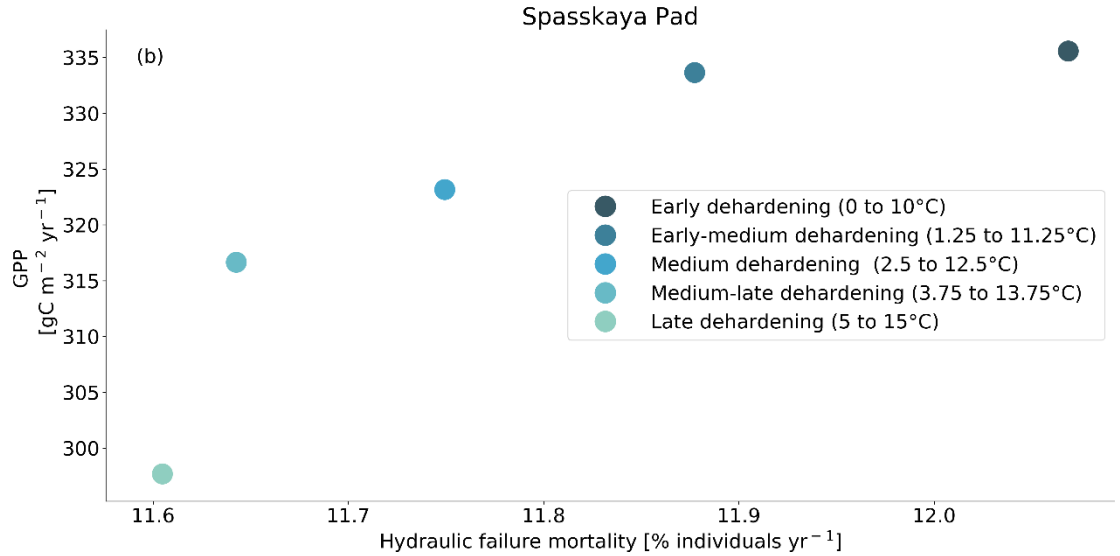

Figure S6: Trade-off between hydraulic failure mortality and gross primary productivity for evergreen needleleaf trees at Spasskaya Pad for 5 dehardening sensitivity experiments. The mortality rates are averaged over the 30 year period 1981 to 2011.

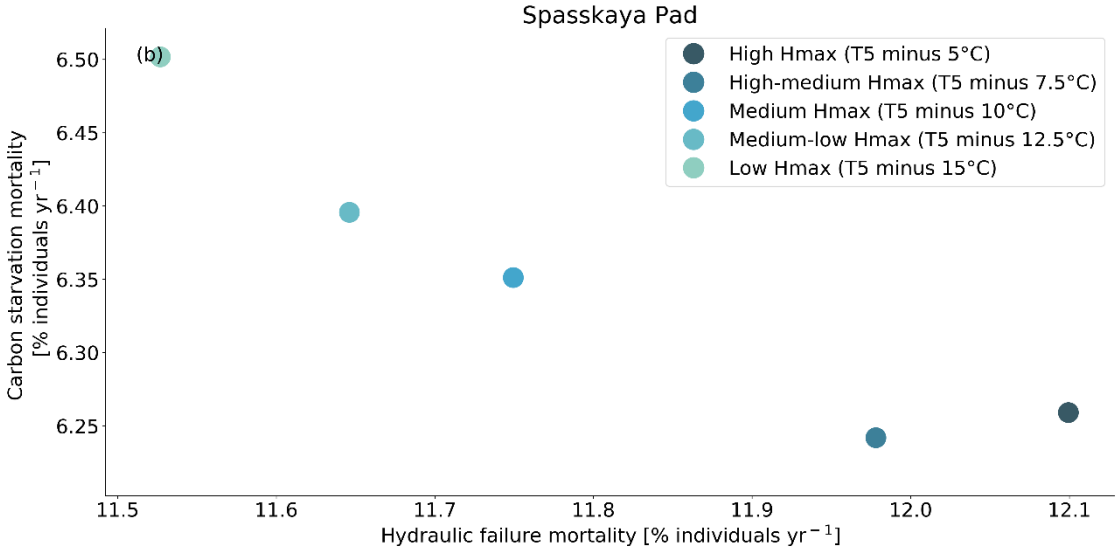

Figure S7: Trade-off between hydraulic failure mortality and carbon starvation mortality for evergreen needleleaf trees at Spasskaya Pad for 5 maximum hardiness level sensitivity experiments. The mortality rates are averaged over the 30 year period 1981 to 2011.

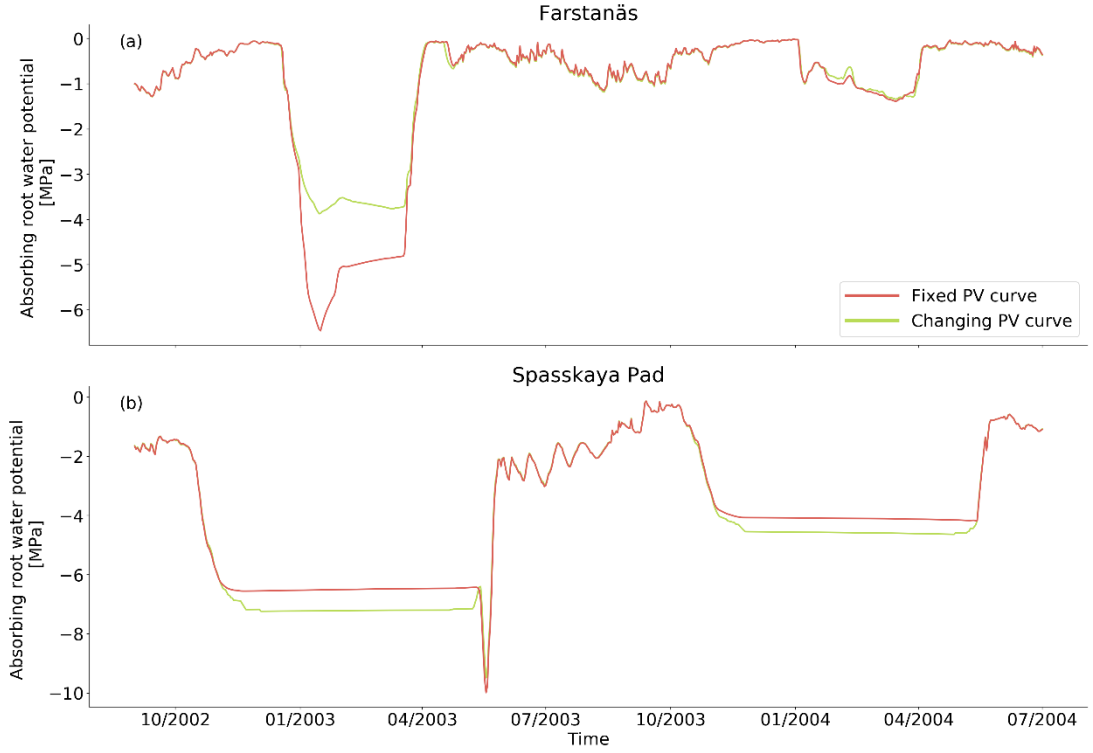

Figure S8: Absorbing root water potential from PV curve sensitivity analysis simulations for needleleaf evergreen trees at the sites of a) Farstanäs, and b) Spasskaya Pad, during the period 2002/09-2004/07.

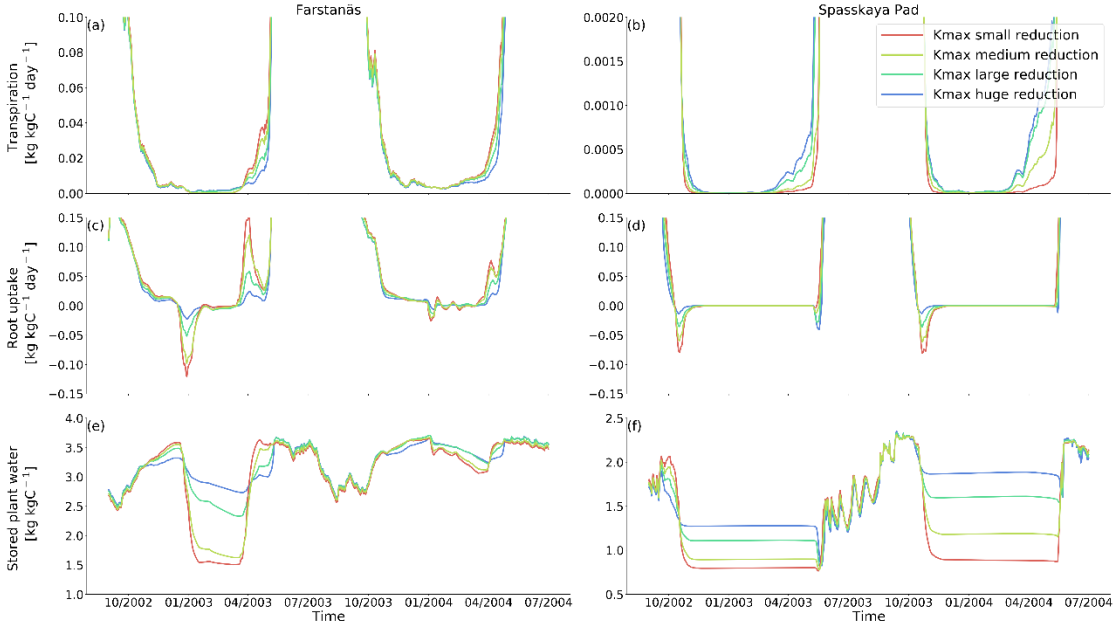

Figure S9: Plant water fluxes from Kmax sensitivity analysis simulations for needleleaf evergreen trees at the sites of: Left) Farstanäs, and Right) Spasskaya Pad, during the period 2002/09-2004/07. Top: transpiration, middle: root water uptake, and bottom: stored plant water.

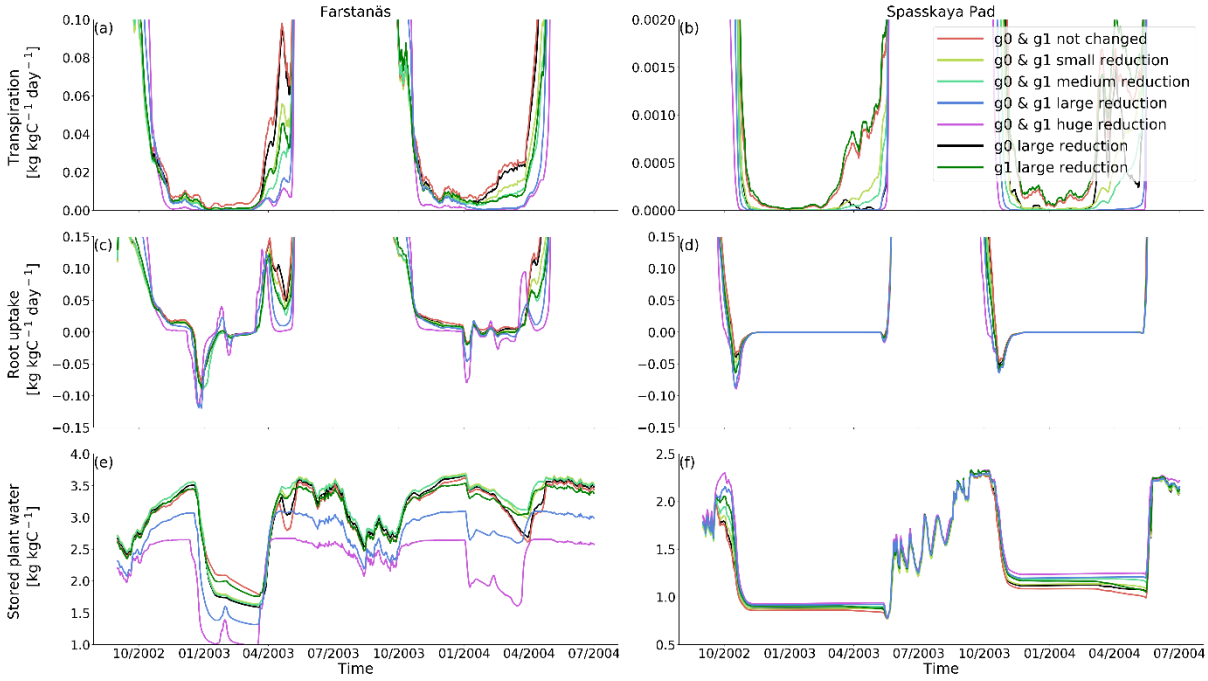

Figure S10: Plant water fluxes from g0 sensitivity analysis simulations for needleleaf evergreen trees at the sites of: Left) Farstanäs, and Right) Spasskaya Pad, during the period 2002/09-2004/07. Top: transpiration, middle: root water uptake, and bottom: stored plant water.

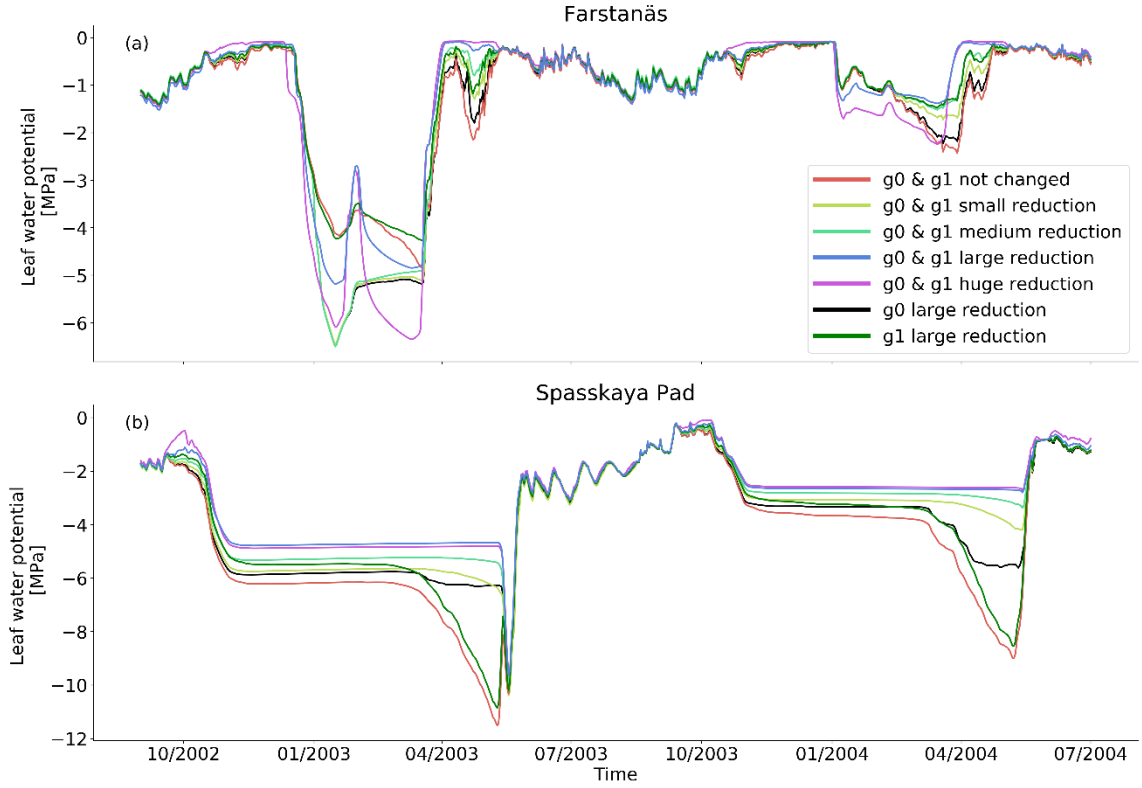

Figure S11: Leaf water potential from g0 sensitivity analysis simulations for needleleaf evergreen trees at the sites of a) Farstanäs, and b) Spasskaya Pad, during the period 2002/09-2004/07.

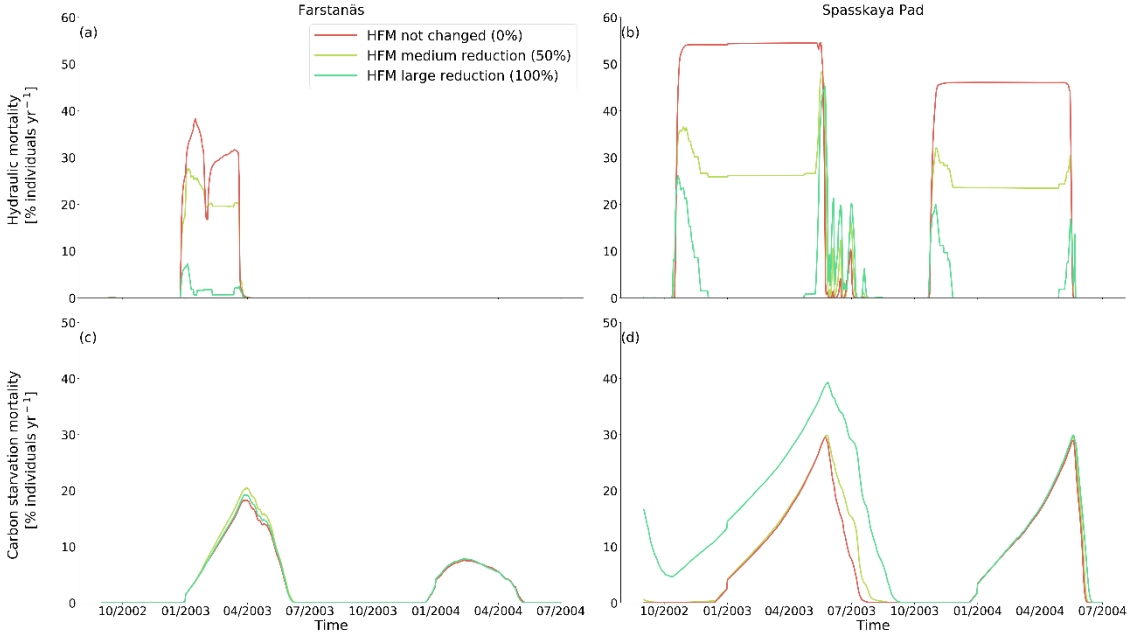

Figure S12: Mortality rates from hydraulic failure mortality sensitivity analysis simulations for needleleaf evergreen trees at the sites of: Left) Farstanäs, and Right) Spasskaya Pad, during the period 2002/09-2004/07. Top: hydraulic failure mortality, and bottom: carbon starvation mortality.

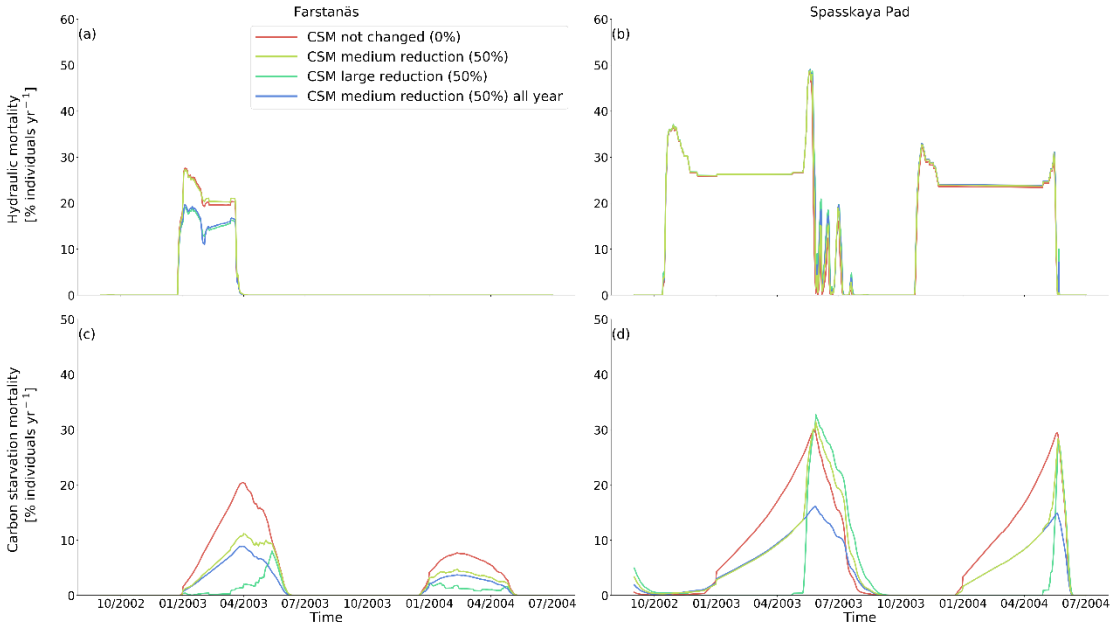

Figure S13: Carbon starvation mortality rate from carbon starvation mortality sensitivity analysis simulations for needleleaf evergreen trees at the sites of a) Farstanäs, and b) Spasskaya Pad, during the period 2002/09-2004/07.